Open Ceramics 17 (2024) 100538

Contents lists available at ScienceDirect

Open Ceramics

journal homepage: www.sciencedirect.com/journal/open-ceramics

Stoichiometric Cr_2AlC MAX phase coatings deposited by HPPMS from composite targets using industrial deposition technology

Yu-Ping Chien [a,*], Stanislav Mráz [a], Clio Azina [a], Szilárd Kolozsvári [b], Peter Polcik [b], Jochen M. Schneider [a]

[a] Materials Chemistry, RWTH Aachen University, Kopernikusstr. 10, D-52074, Aachen, Germany
[b] Plansee Composite Materials GmbH, Siebenbürgerstr. 23, D-86983, Lechbruck am See, Germany

ARTICLE INFO

Handling Editor: Dr P Colombo

Keywords:
Magnetron sputtering
Substrate rotation
HIPIMS
Cr_2AlC MAX phase
Thin films

ABSTRACT

Compositionally-graded Cr_2AlC coatings were deposited from composite targets with Al concentration gradients along the long-axis of the targets, ranging from 20.0 to 30.0 at.%, in an industrial plant. Stoichiometric Cr_2AlC coatings deposited by HPPMS with a peak-power density of 217 W/cm^2 and at substrate bias potential of −100 V require an Al concentration in the target of 30.0 at.% to compensate for the Al-loss induced by preferential re-sputtering and thermally induced desorption at these deposition conditions. The HPPMS deposition of a stoichiometric Cr_2AlC coating at floating potential can be attained from a target segment containing 26.4 at.% of Al. Hence, during synthesis at 560 °C in an industrial deposition system with two-fold rotation significant deviations between target and coating composition were observed. It was demonstrated that these ion energy and power density induced reductions in Al concentration can be compensated for by utilizing Al-rich composite targets.

1. Introduction

Cr_2AlC is a $M_{n+1}AX_n$ phase, where M stands for an early transition metal, A mostly represents groups 13 and 14 elements, X is either C or N, and n ranges from 1 to 3 [1]. These ternary carbides and nitrides, possessing hexagonal nanolaminated crystal structure, consist of alternating metallic-like bonds between M-A layers and ionic/covalent-like bonds between M-X layers [1–3]. Cr_2AlC exhibits electrical and thermal conductivities comparable to stainless steels [4–6] as well as high temperature oxidation resistance [7] comparable to MoAlB [7,8] and hence oxidizes at a much slower rate than ZrB_2 [7,9]. Specifically, the scale thickness after oxidation at 1300 °C for 5 h on MoAlB [8] and ZrB_2 [9] is 6 μm and 180 μm, respectively. Cr_2AlC shows an oxide scale thickness of approximately 6 μm after oxidation at 1320 °C for 4 h and 42 min [7] and is hence in terms of the oxidation behavior similar to MoAlB [7,8]. Due to the above discussed combination of metallic and ceramic properties, Cr_2AlC coatings have been investigated for application as protective coatings in harsh environments such as accident tolerant fuel cladds (ATF) [10–13], bond-coats in thermal barrier coatings (TBCs) [14–17], and concentrated solar power receivers [18,19].

Physical vapor deposition (PVD) of Cr_2AlC coatings has been reported from elemental targets [20] as well as from multi-element compound and/or composite targets [21]. The latter processing strategy is often preferred during industrial-scale processing as the inherent spatial composition variation caused by co-sputtering from multiple elemental targets is prevented. A two- or three-fold substrate rotation is generally used in industrial processes to maximize productivity and coating uniformity. However, chemical composition deviations between the multi-element compound/composite targets and the corresponding magnetron sputtered coatings have been observed for Cr–Al–C [22,23] as well as for other ceramic coating materials such as Ti–B [24], Mo_2BC [25], TaB_2 [26,27], NbC [28], Ti_3SiC_2 [29], Zr–Al–C [30], and Hf-Al-C [30]. Compared to direct current magnetron sputtering (DCMS), typically operating at a power density of several W/cm^2, high power pulsed magnetron sputtering (HPPMS) plasma contains a higher fraction of ionized coating-forming species due to the utilization of significantly higher target power densities of the order of kW/cm^2 [31]. Applying a substrate bias potential lower than −100 V during HPPMS processing results in formation of a significant amount of the disorder solid solution $(Cr,Al)_2C_x$, which deteriorates the mechanical properties of the as deposited coatings [32]. Besides, changing the substrate bias potential from floating to −400 V, during HPPMS deposition from a

* Corresponding author.
E-mail addresses: chien@mch.rwth-aachen.de (Y.-P. Chien), mraz@mch.rwth-aachen.de (S. Mráz), azina@mch.rwth-aachen.de (C. Azina), Szilard.Kolozsvari@plansee.com (S. Kolozsvári), Peter.Polcik@plansee.com (P. Polcik), schneider@mch.rwth-aachen.de (J.M. Schneider).

https://doi.org/10.1016/j.oceram.2024.100538
Received 8 November 2023; Received in revised form 19 December 2023; Accepted 5 January 2024
Available online 6 January 2024
2666-5395/© 2024 The Authors. Published by Elsevier Ltd on behalf of European Ceramic Society. This is an open access article under the CC BY-NC-ND license (http://creativecommons.org/licenses/by-nc-nd/4.0/).

close-to-stoichiometric Cr_2AlC powder metallurgical composite target, resulted in an Al deficiency in the as-deposited coating of up to 20 at.% [23]. It could be shown that this is caused by thermally induced desorption of Al and preferential re-sputtering of Al during growth [23]. Therefore, the working hypothesis is that the Al concentration loss observed during HPPMS processing can be compensated for by employing targets with an Al concentration >25 at. %.

To this end, we study the effects of the target peak power density and substrate bias potential on the chemical composition, phase formation, microstructure evolution, and mechanical properties of the Cr_2AlC coatings deposited by DCMS and HPPMS with two-fold substrate rotation in an industrial, four cathode, deposition system.

2. Experimental details

Cr_2AlC coatings were deposited by magnetron sputtering in an industrial coater, (CemeCon CC 800/9). Four powder metallurgically fabricated composite split $Cr_{0.438}Al_{0.30}C_{0.262}/Cr_{0.50}Al_{0.20}C_{0.30}$ targets with a size of 500 × 88 mm^2 (Plansee Composite Materials GmbH) were used in this study. Cemented carbide substrates (Co-WC) with a dimension of 12.5 × 12.5 × 3 mm^3 were fixed on a cylindrical tower with a radius of 6.75 cm at a distance of 10.55 cm from the target resulting in a minimum target-to-substrate distance of 3.5 cm which can be seen in Fig. 1. Two-fold rotation with a carousel rotation speed of approximately 3 rpm was used.

The substrates were heated to 560 °C and the base pressure with heated substrates was <1.0 mPa prior to all depositions. During sputtering, 200 sccm Ar gas flow was introduced into the coater leading to a deposition pressure of approximately 380 mPa. The time-averaged power input onto each target was set to 1000 W. In the DCMS process the target power density was 2.3 W/cm^2. In HPPMS process, utilizing 50 μs long pulses with 2450 μs pulse-off-time, corresponding to a frequency of 400 Hz and a duty cycle of 2.0 % resulted in a target peak power density of 217 W/cm^2. While the pulse-on period was based on [23,32] a shorter pulse-off period of 2450 μs was chosen to obtain stable plasma processing conditions at maximized target peak power density. Substrate bias potentials, floating and −100 V, were either applied constantly for DCMS or by synchronized 200 μs long pulses during HPPMS. The deposition times for the DCMS and HPPMS processes were 150 and 300 min, respectively.

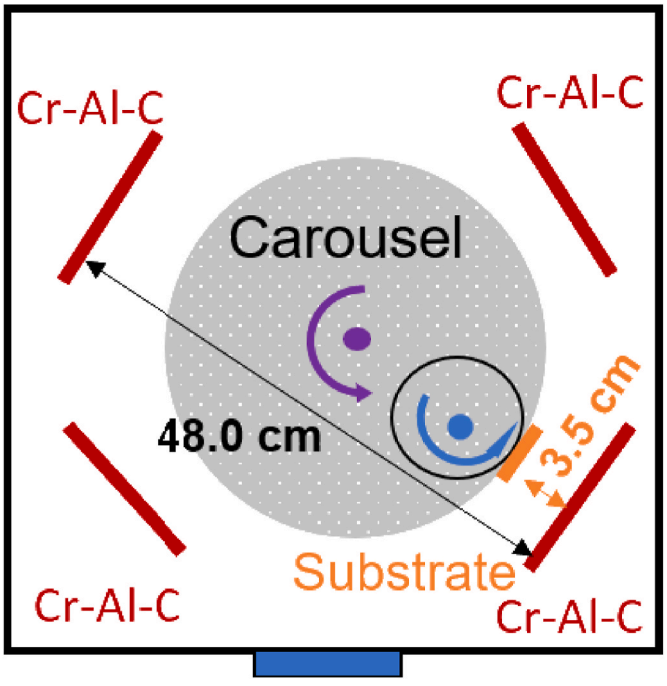

Fig. 1. Schematic representation of the setup utilized for coating deposition with two-fold substrate rotation in an industrial coater utilizing all four cathodes.

The chemical composition of the coatings onto cemented carbide substrates was measured with a Hitachi TM4000Plus scanning electron microscope (SEM), equipped with a Bruker Quantax75 energy dispersive X-ray spectroscopy (EDX) detector, at an acceleration voltage of 15 kV. A standard characterized by time-of-flight elastic recoil detection analysis (ToF-ERDA) and elastic backscattering spectrometry (EBS) was utilized for the composition measurements. The chemical composition of the Cr–Al–C standard was Cr: 49.9 ± 2.5, Al: 24.9 ± 1.2, C: 24.7 ± 1.2, O: 0.5 ± 0.3 at.%. The measurement conditions can be found elsewhere [33].

Grazing incidence X-ray diffraction (GiXRD) analysis of the deposited coatings was carried out using a PANalytical Empyrean diffractometer with a Cu Kα radiation source (λ = 1.540598 Å). The diffractometer was operated with an incidence angle of 1° using a step size of 0.015° and scanning time of 2 s per step.

The film microstructure was investigated using scanning transmission electron microscopy (STEM) on thin lamellae that were prepared by focused ion beam (FIB) using a FEI Helios NanoLab 660 dual-beam microscope with Ga^+ ions accelerated at 30 kV. A STEM III detector was used in bright field (BF) mode for imaging with a voltage and current of 30 kV and 100 pA, respectively. The topography was studied by scanning electron microscopy (SEM) with a voltage and current of 10 kV and 100 pA.

Nanoindentation was conducted in a Hysitron TI-900 TriboIndenter and the Young's modulus of each film was determined by the Oliver-Pharr method [34]. A maximum force of 5 mN operated in load-controlled mode with a Berkovich diamond tip generated a contact depth of <10 % of the coating thickness. At least 54 indentation measurements were carried out for each sample and the tip area function was determined with a fused silica standard. A Poisson's ratio of 0.188 was used for Cr_2AlC [5].

3. Results and discussion

Fig. 2 shows a schematic of the here utilized split composite target and the measured chemical composition profiles of Cr–Al–C coatings onto cemented carbide substrates deposited by DCMS and HPPMS along the long axis of the targets. The yellow regions mark the positions where, within the measurement uncertainties, stoichiometric coating compositions were obtained. It is evident that the actual locations where stoichiometric coatings can be synthesized, strongly depend on the deposition conditions and that they are moved toward the Al-rich end of the targets as the power density and ion energy is increased.

As discussed above, the Al-deficiency in Cr–Al–C coatings is caused by preferential Al re-sputtering and thermally induced desorption [23]. Both effects are enhanced during HPPMS due to higher energy and ion fluxes compared to DCMS [23]. Therefore, targets providing an Al excess (Al concentration >25 at.%) were utilized in an attempt to compensate for the Al-loss caused by these two mechanisms. It is demonstrated that the chemical composition deviations of the coatings can be compensated for based on utilizing off-stoichiometric target compositions for the growth of stoichiometric thin films. For example, an Al target concentration of 30 at.% compensated the Al loss during HPPMS at a substrate bias potential of −100 V, resulting in the deposition of a stoichiometric Cr_2AlC coating. For the HPPMS coating deposited at floating potential, target segments containing 26.4 at.% Al are required, while for DCMS at floating potential no Al excess is required. The chemical composition of the, within the measurement uncertainties, stoichiometric Cr_2AlC coatings are summarized in Table 1 for the corresponding deposition conditions.

The diffractograms of the stoichiometric Cr_2AlC coatings deposited by DCMS and HPPMS are shown in Fig. 3. While the characteristic (002)

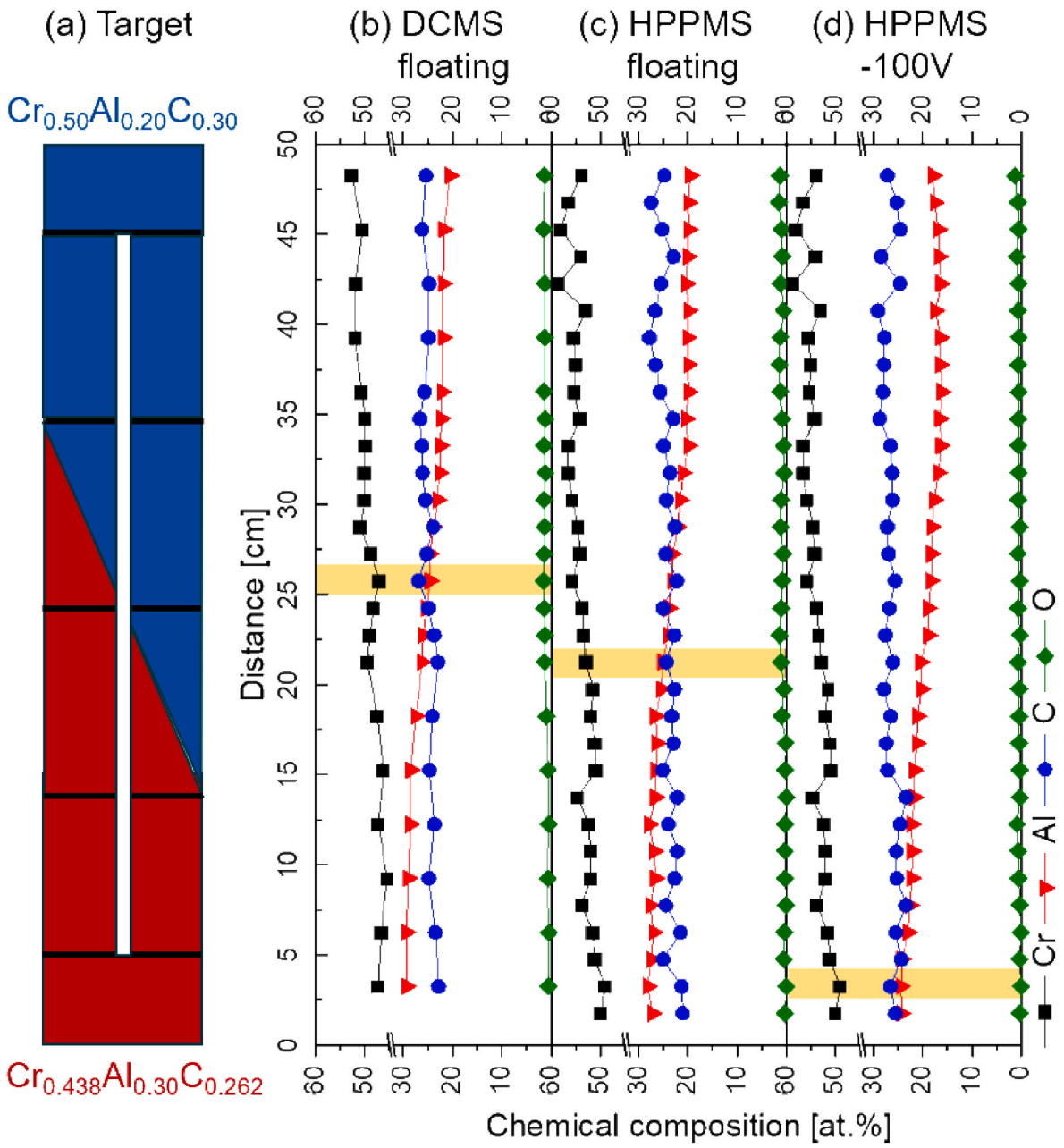

Fig. 2. (a) Schematic of the split composite target geometry utilized here and the chemical composition profiles measured by EDX for coatings deposited by DCMS at floating substrate bias potential (b) as well as by HPPMS at substrate bias potentials of floating (c) and −100 V (d).

Table 1
Chemical compositions determined by EDX of the coatings from Fig. 1 within the regions marked in yellow.

	Cr [at. %]	Al [at. %]	C [at. %]	O [at. %]
DCMS floating	47.0 ± 2.4	24.6 ± 1.2	26.9 ± 1.3	1.5 ± 0.8
HPPMS floating	49.5 ± 2.5	25.1 ± 1.3	24.3 ± 1.2	1.0 ± 0.5
HPPMS -100 V	49.0 ± 2.5	24.4 ± 1.2	26.5 ± 1.3	0.1 ± 0.1

basal plane peak at 13.8° is not visible in the diffraction geometry employed here, the equally characteristic (101) peak at 36.9° is observed in all coatings, indicating the formation of the Cr_2AlC MAX phase. The formation temperature, 560 °C, of Cr_2AlC coatings deposited with 2-fold substrate rotation is similar to previous reports using stationary deposition geometry [35].

The cross-sectional scanning transmission electron microscopy (STEM) images of the coatings deposited by DCMS and HPPMS are shown in Fig. 4. The morphology of all coatings is V-shaped columnar as illustrated by the yellow lines. The bright areas indicated the presence of intercolumnar pores, as indicated by red arrows. As can be clearly observed in Fig. 4b and c, the pore size and number density are reduced in the coatings deposited by HPPMS compared to the DCMS deposition. Compared to DCMS, the HPPMS plasma consists of a large fraction of ionized coating-forming species [23] with energies up to several tens of eV [36]. The larger ion flux and ion energy triggers surface diffusion, which results in finer columnar grains and coating densification [23, 36–38]. The deposition rate for DCMS and HPPMS processing, both operating with a time averaged power of 1000 W, is 1.68 and 1.12 μm/h, respectively. Hence, the HPPMS deposition rate is about 33 % lower than for DCMS. Deposition rate reduction of 38 % was reported for depositions from a Cr_2AlC compound target onto stationary substrates with similar time averaged power density, 5.6 W/cm^2 (target peak

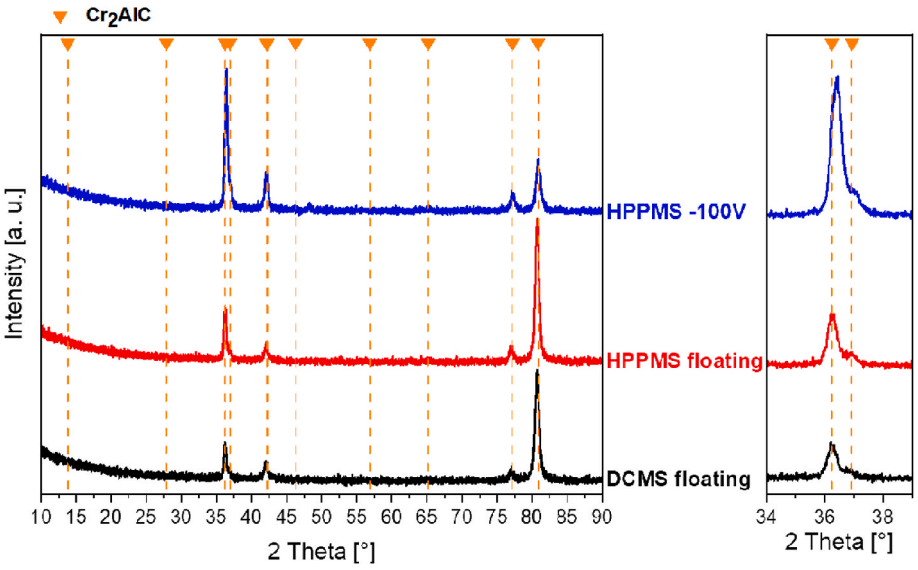

Fig. 3. Grazing incidence X-ray diffractograms of Cr_2AlC coatings deposited by DCMS and HPPMS and a close-up of characteristic peaks of the MAX phase: (100) at 36.236°, and (101) at 36.930°. Reference positions are taken from card (00-029-0017) of the International Centre for Diffraction Data.

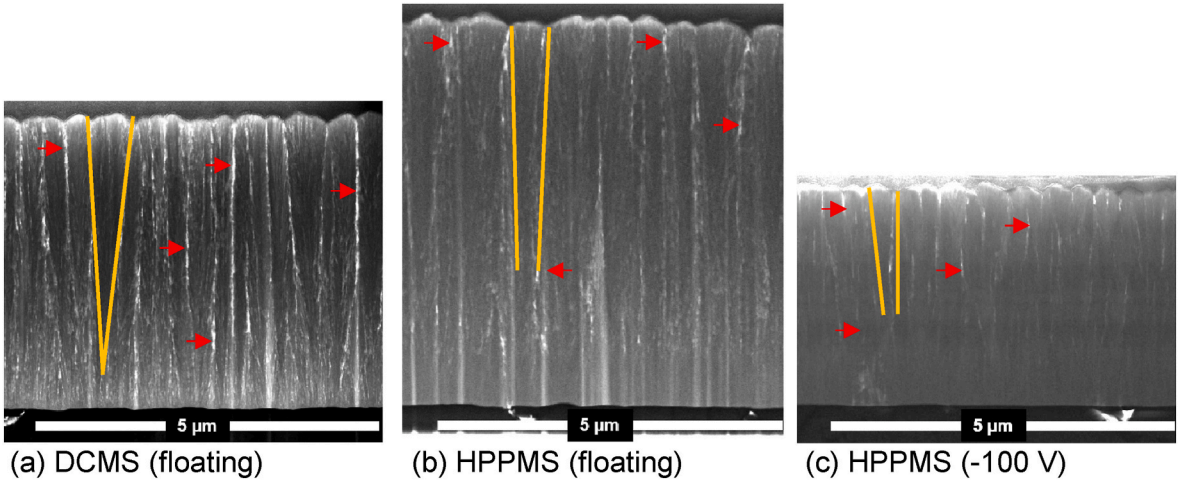

Fig. 4. Cross-sectional bright field (BF) scanning transmission electron microscopy (STEM) images of Cr_2AlC coatings deposited using DCMS at (a) floating for 150 min and HPPMS at (b) floating and (c) −100 V substrate bias potential for 300 min. The yellow lines and red arrows marked the columnar grains and intercolumnar pores, respectively. (For interpretation of the references to colour in this figure legend, the reader is referred to the Web version of this article.)

power density = 300.5 W/cm^2) for HPPMS and 5.7 W/cm^2 for DCMS processing, respectively [39]. Hence, the deposition rate reduction reported in Ref. [39] is comparable to the here reported data. As the substrate bias potential of −100 V is applied during HPPMS processing, the deposition rate drops to 0.63 µm/h. The reasons for this 44 % reduction are besides the inhomogeneous distribution of thickness of the

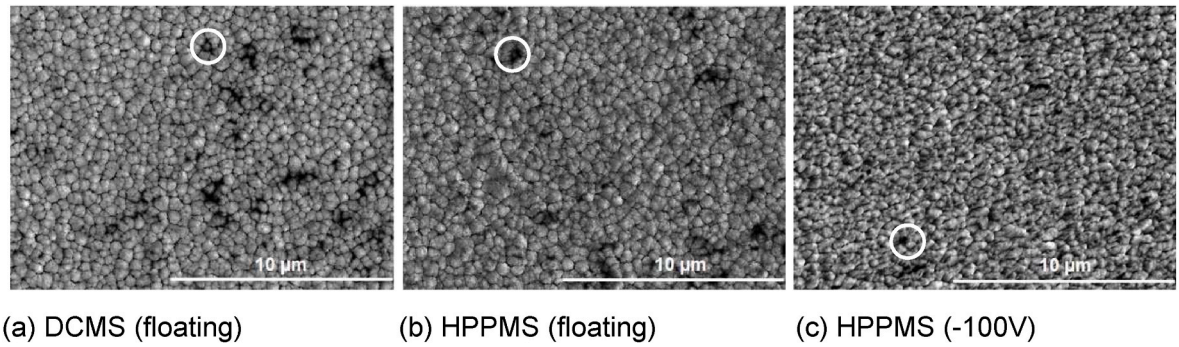

Fig. 5. SEM images of the topography of Cr_2AlC coatings deposited using DCMS at (a) floating and HPPMS at (b) floating and (c) −100 V substrate bias potential. The white circles marked the pores on the surface.

coatings along the target long axis, also re-sputtering and thermally induced desorption [23].

Fig. 5 shows the SEM top view micrographs of the as-deposited coatings. The topography is facetted consistent with the columnar grain morphology visible in Fig. 4. Furthermore, under-dense regions are marked by white circles, see Fig. 5.

The Young's moduli of Cr_2AlC coatings deposited by DCMS at floating substrate bias potential and HPPMS were determined by nanoindentation and are shown in Fig. 6. The DCMS coating shows an average Young's modulus of 248 ± 33 GPa. The average modulus of HPPMS coatings increases from 281 ± 39 GPa at floating to 296 ± 33 GPa at −100 V substrate bias potential, which is 16 % lower than the calculated DFT values of 349 GPa [32]. This difference is according to Paier within the expected deviation of the here employed functionals [40] and the experimental nanoindentation data [41]. The modulus of the HPPMS deposited columnar coating using a substrate bias potential of −100 V is in good agreement with the 298 ± 21 GPa value reported for a Cr_2AlC coating deposited by DCMS at 650 °C in a stationary geometry [21]. The 19 % lower Young's modulus measured for the DCMS coating compared to the HPPMS coating deposited at −100 V substrate bias potential can be attributed to the porosity visible between the column boundaries in Fig. 4a. Recently, Fekete et al. reported a Young's modulus measurement of 341 ± 9 GPa for a Cr_2AlC coating which was annealed to 690 °C exhibiting a dense, equiaxed microstructure [5]. The deviation of the measured Young's modulus to the ab initio predicted value [32] is 2 % and hence theory and experiment are in excellent agreement, underlining the detrimental effect of the aforementioned inter-columnar porosity on the elastic modulus.

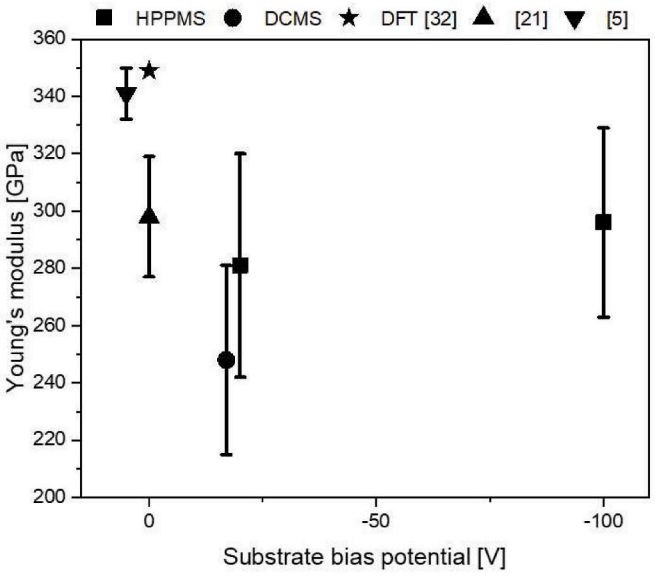

Fig. 6. Young's moduli of the Cr_2AlC coatings deposited by DCMS and HPPMS determined by nanoindentation. For comparison, DFT (300 K) data for Cr_2AlC MAX phase from Ref. [32] and other Cr_2AlC coatings in the literature [5,21] are presented.

4. Conclusions

Following the working hypothesis that for the deposition of stoichiometric Cr_2AlC coatings non-stoichiometric targets are required, four powder metallurgical composite Cr–Al–C targets with Al concentration gradients ranging from 20.0 to 30.0 at.% were employed in an industrial plant using two-fold substrate rotation. It was demonstrated that the excess Al in the target can compensate for the Al-loss induced by preferential Al re-sputtering triggered by ion bombardment and thermal desorption at a substrate temperature of 560 °C. The HPPMS coating deposited at a substrate bias potential of −100 V requires 30.0 at.% Al, i.e. a 5 at.% Al excess in the target to attain stoichiometry in the film. In addition, the coating deposited at this condition shows an elastic modulus which is consistent with ab initio predictions and with measured elastic moduli of coatings deposited without substrate rotation. From the here communicated data it is evident that the target composition required to ensure the deposition of stoichiometric Cr_2AC coatings is crucially dependent on both power density and substrate bias potential. Hence, target compositions can only be optimized for a certain set of deposition conditions as target power density, substrate bias potential as well as substrate temperature affect the magnitudes of Al re-sputtering and Al evaporation during growth.

Author contributions

Conceptualization, Y.-P.C., S.M., J.M.S.; methodology, Y.-P.C., S.M., C.A., J.M.S.; validation, Y.-P.C., C.A., and J.M.S.; formal analysis, Y.-P.C., C.A.; investigation, Y.-P.C., C.A.; resources, S.K., P.P.; data curation, Y.-P.C..; writing—original draft preparation, Y.-P.C.; writing—review and editing, S.M., C.A., S.K., P.P., J.M.S.; visualization, Y.-P.C., S.M., C.A.; supervision, J.M.S.; project administration, J.M.S.; funding acquisition, J.M.S.

Funding

This research was funded by German Research Foundation (DFG, SFB-TR 87/3) "Pulsed high power plasmas for the synthesis of nanostructured functional layers".

Data availability statement

The data presented in this study are available on request from the corresponding author.

Declaration of competing interest

The authors declare that they have no known competing financial interests or personal relationships that could have appeared to influence the work reported in this paper.

Acknowledgements

The authors would like to thank G. Fidanboy for performing the nanoindentation measurements and Prof. Daniel Primetzhofer from Uppsala University for characterization of the Cr–Al–C standard sample by ToF-ERDA and EBS.

References

[1] M.W. Barsoum, MAX Phases: Properties of Machinable Ternary Carbides and Nitrides, John Wiley & Sons, 2013.
[2] M. Baben, L. Shang, J. Emmerlich, J.M. Schneider, Oxygen incorporation in M2AlC (M=Ti, V, Cr), Acta Mater. 60 (12) (2012) 4810–4818, https://doi.org/10.1016/j.actamat.2012.05.011.
[3] J.M. Schneider, Z. Sun, R. Mertens, F. Uestel, R. Ahuja, Ab initio calculations and experimental determination of the structure of Cr2AlC, Solid State Commun. 130 (7) (2004) 445–449, https://doi.org/10.1016/j.ssc.2004.02.047.
[4] J.D. Hettinger, S.E. Lofland, P. Finkel, T. Meehan, J. Palma, K. Harrell, S. Gupta, A. Ganguly, T. El-Raghy, M.W. Barsoum, Electrical transport, thermal transport, and elastic properties ofM2AlC(M=Ti, Cr, Nb, and V), Phys. Rev. B 72 (11) (2005), https://doi.org/10.1103/PhysRevB.72.115120.
[5] M. Fekete, C. Azina, P. Ondračka, L. Löfler, D. Bogdanovski, D. Primetzhofer, M. Hans, J.M. Schneider, On the determination of the thermal shock parameter of MAX phases: a combined experimental-computational study, J. Eur. Ceram. Soc. 43 (13) (2023) 5484–5492, https://doi.org/10.1016/j.jeurceramsoc.2023.05.007.
[6] T. Chu, C. Ho, Thermal conductivity and electrical resistivity of eight selected AISI stainless steels, Therm. Conduct. 15 (1978) 79–104, https://doi.org/10.1007/978-1-4615-9083-5_12.
[7] D.E. Hajas, M. to Baben, B. Hallstedt, R. Iskandar, J. Mayer, J.M. Schneider, Oxidation of Cr2AlC coatings in the temperature range of 1230 to 1410°C, Surf. Coat. Technol. 206 (4) (2011) 591–598, https://doi.org/10.1016/j.surfcoat.2011.03.086.

[8] S. Kota, E. Zapata-Solvas, A. Ly, J. Lu, O. Elkassabany, A. Huon, W.E. Lee, L. Hultman, S.J. May, M.W. Barsoum, Synthesis and characterization of an alumina forming nanolaminated boride: MoAlB, Sci. Rep. 6 (2016) 26475. https://10.1038/srep26475.
[9] M.M. Opeka, I.G. Talmy, E.J. Wuchina, J.A. Zaykoski, S.J. Causey, Mechanical, thermal, and oxidation properties of refractory hafnium and zirconium compounds, J. Eur. Ceram. Soc. 19 (13–14) (1999) 2405–2414, https://doi.org/10.1016/S0955-2219(99)00129-6.
[10] M. Ougier, A. Michau, F. Lomello, F. Schuster, H. Maskrot, M.L. Schlegel, High-temperature oxidation behavior of HiPIMS as-deposited Cr–Al–C and annealed Cr2AlC coatings on Zr-based alloy, J. Nucl. Mater. 528 (2020) 151855, https://doi.org/10.1016/j.jnucmat.2019.151855.
[11] S. Mráz, M. Tyra, M. to Baben, M. Hans, X. Chen, F. Herrig, K. Lambrinou, J. M. Schneider, Thermal stability enhancement of Cr2AlC coatings on Zr by utilizing a double layer diffusion barrier, J. Eur. Ceram. Soc. 40 (4) (2020) 1119–1124, https://doi.org/10.1016/j.jeurceramsoc.2019.10.008.
[12] C. Tang, M. Große, S. Ulrich, M. Klimenkov, U. Jäntsch, H.J. Seifert, M. Stüber, M. Steinbrück, High-temperature oxidation and hydrothermal corrosion of textured Cr2AlC-based coatings on zirconium alloy fuel cladding, Surf. Coat. Technol. 419 (2021) 127263, https://doi.org/10.1016/j.surfcoat.2021.127263.
[13] E. Charalampopoulou, K. Lambrinou, T. Van der Donck, B. Paladino, F. Di Fonzo, C. Azina, P. Eklund, S. Mráz, J.M. Schneider, D. Schryvers, Early stages of dissolution corrosion in 316L and DIN 1.4970 austenitic stainless steels with and without anticorrosion coatings in static liquid lead-bismuth eutectic (LBE) at 500 C, Mater. Char. 178 (2021) 111234, https://doi.org/10.1016/j.matchar.2021.111234. %@ 1044-5803.
[14] J. Gonzalez-Julian, G. Mauer, D. Sebold, D.E. Mack, R. Vassen, Cr2AlC MAX phase as bond coat for thermal barrier coatings: processing, testing under thermal gradient loading, and future challenges, J. Am. Ceram. Soc. 103 (4) (2020) 2362–2375, https://doi.org/10.1111/jace.16935.
[15] M. Sokol, J. Yang, H. Keshavan, M.W. Barsoum, Bonding and oxidation protection of Ti2AlC and Cr2AlC for a Ni-based superalloy, J. Eur. Ceram. Soc. 39 (4) (2019) 878–882, https://doi.org/10.1016/j.jeurceramsoc.2018.10.019.
[16] T. Go, Y. Sohn, G. Mauer, R. Vaßen, J. Gonzalez-Julian, Cold spray deposition of Cr2AlC MAX phase for coatings and bond-coat layers, J. Eur. Ceram. Soc. 39 (4) (2019) 860–867, https://doi.org/10.1016/j.jeurceramsoc.2018.11.035.
[17] J. Gonzalez-Julian, T. Go, D. Mack, R. Vaßen, Thermal cycling testing of TBCs on Cr2AlC MAX phase substrates, Surf. Coat. Technol. 340 (2018) 17–24, https://doi.org/10.1016/j.surfcoat.2018.02.035.
[18] C. Azina, S. Badie, A. Litnovsky, L. Silvestroni, E. Sani, J. Gonzalez-Julian, Optical properties and corrosion resistance of Ti2AlC, Ti3AlC2, and Cr2AlC as candidates for concentrated solar power receivers, Sol. Energy Mater. Sol. Cell. 259 (2023) 112433, https://doi.org/10.1016/j.solmat.2023.112433.
[19] J. Sarwar, T. Shrouf, A. Srinivasa, H. Gao, M. Radovic, K. Kakosimos, Characterization of thermal performance, flux transmission performance and optical properties of MAX phase materials under concentrated solar irradiation, Sol. Energy Mater. Sol. Cell. 182 (2018) 76–91, https://doi.org/10.1016/j.solmat.2018.03.018.
[20] R. Mertens, Z. Sun, D. Music, J.M. Schneider, Effect of the composition on the structure of Cr-Al-C investigated by combinatorial thin film synthesis and ab initio calculations, Adv. Eng. Mater. 6 (11) (2004) 903–907, https://doi.org/10.1002/adem.200400096.
[21] J.M. Schneider, D.P. Sigumonrong, D. Music, C. Walter, J. Emmerlich, R. Iskandar, J. Mayer, Elastic properties of Cr2AlC thin films probed by nanoindentation and ab initio molecular dynamics, Scripta Mater. 57 (12) (2007) 1137–1140, https://doi.org/10.1016/j.scriptamat.2007.08.006.
[22] S. Mráz, J. Emmerlich, F. Weyand, J.M. Schneider, Angle-resolved evolution of the composition of Cr–Al–C thin films deposited by sputtering of a compound target, J. Phys. D Appl. Phys. 46 (13) (2013) 135501, https://doi.org/10.1088/0022-3727/46/13/135501.
[23] H. Rueß, M. to Baben, S. Mráz, L. Shang, P. Polcik, S. Kolozsvári, M. Hans, D. Primetzhofer, J.M. Schneider, HPPMS deposition from composite targets: effect of two orders of magnitude target power density changes on the composition of sputtered Cr-Al-C thin films, Vacuum 145 (2017) 285–289, https://doi.org/10.1016/j.vacuum.2017.08.048.
[24] J. Neidhardt, S. Mráz, J.M. Schneider, E. Strub, W. Bohne, B. Liedke, W. Möller, C. Mitterer, Experiment and simulation of the compositional evolution of Ti–B thin films deposited by sputtering of a compound target, J. Appl. Phys. 104 (6) (2008) 063304, https://doi.org/10.1063/1.2978211.
[25] J.-O. Achenbach, S. Mráz, D. Primetzhofer, J. Schneider, Correlative experimental and theoretical investigation of the angle-resolved composition evolution of thin films sputtered from a compound Mo2BC target, Coatings 9 (3) (2019) 206, https://doi.org/10.3390/coatings9030206.
[26] V. Šroba, T. Fiantok, M. Truchlý, T. Roch, M. Zahoran, B. Grančič, P. Švec, Š. Nagy, V. Izai, P. Kúš, M. Mikula, Structure evolution and mechanical properties of hard tantalum diboride films, J. Vac. Sci. Technol. A 38 (3) (2020) 033408, https://doi.org/10.1116/6.0000155.
[27] K. Viskupová, B. Grančič, T. Roch, L. Satrapinskyy, M. Truchlý, M. Mikula, V. Šroba, P. Ďurina, P. Kúš, Effect of reflected Ar neutrals on tantalum diboride coatings prepared by direct current magnetron sputtering, Surf. Coat. Technol. 421 (2021) 127463, https://doi.org/10.1016/j.surfcoat.2021.127463.
[28] M.Y. Liao, Y. Gotoh, H. Tsuji, J. Ishikawa, Compound-target sputtering for niobium carbide thin-film deposition, J. Vac. Sci. Technol. B 22 (5) (2004) L24, https://doi.org/10.1116/1.1800491.
[29] P. Eklund, M. Beckers, J. Frodelius, H. Högberg, L. Hultman, Magnetron sputtering of Ti3SiC2 thin films from a compound target, J. Vac. Sci. Technol. A 25 (5) (2007) 1381, https://doi.org/10.1116/1.2757178.
[30] Y.-P. Chien, S. Mráz, M. Fekete, M. Hans, D. Primetzhofer, S. Kolozsvári, P. Polcik, J.M. Schneider, Deviations between film and target compositions induced by backscattered Ar during sputtering from M2-Al-C (M = Cr, Zr, and Hf) composite targets, Surf. Coat. Technol. 446 (2022) 128764, https://doi.org/10.1016/j.surfcoat.2022.128764.
[31] V. Kouznetsov, K. Macak, J.M. Schneider, U. Helmersson, I. Petrov, A novel pulsed magnetron sputter technique utilizing very high target power densities, Surf. Coat. Technol. 122 (2–3) (1999) 290–293, https://doi.org/10.1016/S0257-8972(99)00292-3.
[32] H. Rueß, J. Werner, Y. Unutulmazsoy, J.W. Gerlach, X. Chen, B. Stelzer, D. Music, S. Kolozsvari, P. Polcik, T.E. Weirich, J.M. Schneider, Effect of target peak power density on the phase formation, microstructure evolution, and mechanical properties of Cr2AlC MAX-phase coatings, J. Eur. Ceram. Soc. 41 (3) (2021) 1841–1847, https://doi.org/10.1016/j.jeurceramsoc.2020.10.072.
[33] B. Stelzer, X. Chen, P. Bliem, M. Hans, B. Volker, R. Sahu, C. Scheu, D. Primetzhofer, J.M. Schneider, Remote tracking of phase changes in Cr2AlC thin films by in-situ resistivity measurements, Sci. Rep. 9 (1) (2019) 8266, https://doi.org/10.1038/s41598-019-44692-4.
[34] W.C. Oliver, G.M. Pharr, An improved technique for determining hardness and elastic modulus using load and displacement sensing indentation experiments, J. Mater. Res. 7 (6) (1992) 1564–1583, https://doi.org/10.1557/JMR.1992.1564.
[35] C. Walter, D.P. Sigumonrong, T. El-Raghy, J.M. Schneider, Towards large area deposition of Cr2AlC on steel, Thin Solid Films 515 (2) (2006) 389–393, https://doi.org/10.1016/j.tsf.2005.12.219.
[36] A. Hecimovic, A.P. Ehiasarian, Time evolution of ion energies in HIPIMS of chromium plasma discharge, J. Phys. D Appl. Phys. 42 (13) (2009) 135209, https://doi.org/10.1088/0022-3727/42/13/135209.
[37] I. Petrov, P.B. Barna, L. Hultman, J.E. Greene, Microstructural evolution during film growth, J. Vac. Sci. Technol. A 21 (5) (2003) S117–S128, https://doi.org/10.1116/1.1601610.
[38] J. Alami, K. Sarakinos, F. Uslu, M. Wuttig, On the relationship between the peak target current and the morphology of chromium nitride thin films deposited by reactive high power pulsed magnetron sputtering, J. Phys. D Appl. Phys. 42 (1) (2009) 015304, https://doi.org/10.1080/21663831.2017.1414081.
[39] M.W. Qureshi, X. Ma, G. Tang, B. Miao, J. Niu, Fabrication and mechanical properties of Cr2AlC MAX phase coatings on TiBw/Ti6Al4V composite prepared by HiPIMS, Materials 14 (4) (2021). https://10.3390/ma14040826.
[40] J. Paier, M. Marsman, K. Hummer, G. Kresse, I.C. Gerber, J.G. Angyan, Screened hybrid density functionals applied to solids, J. Chem. Phys. 124 (15) (2006) 154709, https://doi.org/10.1063/1.2187006.
[41] J.S.K.L. Gibson, S. Rezaei, H. Rueß, M. Hans, D. Music, S. Wulfinghoff, J. M. Schneider, S. Reese, S. Korte-Kerzel, From quantum to continuum mechanics: studying the fracture toughness of transition metal nitrides and oxynitrides, Mater. Res. Lett. 6 (2) (2017) 142–151, https://doi.org/10.1080/21663831.2017.1414081.